Synthesis of superhydrophobic coatings based on silica nanostructure modified with organosilane compounds by sol-gel method for glass surfaces

Mohammad Ghodrati
Semnan University
Mehdi Mousavi-Kamazani (M.Mousavi@semnan.ac.ir)
Semnan University
Zohreh Bahrami
Semnan University

Article

Keywords: Super-hydrophobic coating, Contact angle, StÖber method, Experimental design, Base catalyst

Posted Date: December 6th, 2022

DOI: https://doi.org/10.21203/rs.3.rs-2313425/v1

Additional Declarations: No competing interests reported.

Version of Record: A version of this preprint was published at Scientific Reports on January 11th, 2023.
See the published version at https://doi.org/10.1038/s41598-023-27811-0.

Abstract

In the present study, the superhydrophobic coating was synthesized by spherical silica nanostructures modified with organosilane compounds for glass surfaces. To optimize the conditions in terms of cost-effectiveness and to create a super-hydrophobic coating with a high contact angle, the design of the central composite (CCD) method was performed for the StÖber method and the contact angle was defined as the response. Tetraethoxysilane (TEOS) was used as a precursor and dimethylsiloxane (PDMS) was used to modify the surface of a spherical silica nanostructure synthesized by a one-step sol-gel method using a base catalyst. The accuracy of the research was checked by the contact angle measurement test and an angle of 162 degrees was obtained. XRD, FT-IR, EDS, SEM, DLS, and AFM analyzes were performed to investigate the synthesis of silica nanostructure. chemical resistance was performed in acidic, neutral, and alkaline environments and the contact angles were 127°, 134°, and 90°, respectively, which indicates that the coating created on the surface glass has good chemical resistance in acidic and neutral environments.

1. Introduction

Smart coatings are coatings that automatically respond to changes in the environment such as heat, light, humidity, temperature, pressure, and pH. The purpose of designing such coatings for higher performance is to increase product life and significantly reduce maintenance costs [1–7]. Due to the unique properties of nanoscale materials and the growing demand for nanomaterials in sectors such as the medical and automotive industries, research and development on nano-based coatings replace conventional polymer coatings [8, 9]. Smart coatings are classified based on application, performance, reactivity, level of complexity, and manufacturing methods. Active sensing coatings include corrosion and pressure-sensitive coatings. Flame retardant coatings are penetrating and non-penetrating coatings. Anti-powder and antibacterial coatings are known as activating coatings. Easy-to-clean coatings include self-cleaning and anti-graphite coatings. Smart window coverings are optically active coatings. Other coatings are anti-fingerprint, anti-reflective, anti-freeze, and anti-fog [10]. Ultra-waterproof coatings are an important category of smart coatings that have received a lot of attention due to their properties. These coatings can be used in any of the above coatings due to their unique properties. For example, due to biodegradation, they can be used in self-healing and antibacterial coatings [11–13], due to morphology and size in self-cleaning and anti-corrosion coatings [14–16], and due to their chemical properties in antifreeze and anti-vapor [17, 18].

Superhydrophobic surfaces are known for two important properties, the first is the surface roughness at the micro and nanoscales and the second is the complex structure. Therefore, synthesis methods such as electrochemical deposition [19], CVD [20], layer-by-layer (LBL) deposition [21], hydrothermal [22], and sol-gel can [23] be used to develop and fabricate the mentioned properties. The sol-gel method is divided into hydrolysis and compaction stages. The raw materials used are silane and metal alkoxides. Among the advantages of the sol-gel method are low-temperature synthesis, high purity, precise control of particle size and distribution, and the possibility of making new crystalline and non-crystalline materials [24,25].

Rough surfaces can be created with the help of SiO_2 [26], Al_2O_3 [27], and $CuSO_4$ [28], and with the help of hydrophobic agents such as PDMS [29], HDTMS [30], surfaces with low surface energy can be made.

In this research, Design-Expert software and a central composite design method were used to synthesize a superhydrophobic coating on the glass surface to optimize the StÖber process parameters, and the contact angle of the water droplet and the superhydrophobic coating was selected as the answer. The selected parameters include deionized water as a hydrolyzing agent, ethanol as a solvent, ammonia as a catalyst, and polydimethylsiloxane as a surface modifying agent. In this method, the experimental design is performed by specifying the actual levels and coding levels for each parameter (ie for high levels + 1, central levels zero, and low levels − 1).

2. Experimental

2.1. Materials and instruments

All chemical materials and compounds used in this study, including tetraethyl orthosilicate (TEOS) ($Si(OC_2H_5)_4$), polydimethylsiloxane (PDMS) ($(C_2H_6OSi)_n$), ammonia (NH_3OH), ethanol (C_2H_5OH), and hydrochloric acid (HCl) were purchased from Merck. All chemicals materials used were highly purified and consumed without purification. The contact angle was measured by Jikan CAG-20. XRD (X-ray diffraction) patterns were studied by Philips-X PertPro device using Ni-filtered Cu Kα radiation. FT-IR (Fourier transform infrared) analysis was performed with Magna-IR, spectrometer 550 Nicolet with a resolution of 0.125 cm^{-1} in KBr pellets ranging from 400 to 4000 cm^{-1}. The light transmittance (transparency) by PHYSTEC - UVS 2500 was investigated. EDS (energy dispersion spectroscopy) analysis was performed using a Philips XL30 microscope device. MIRA3 FEG-SEM was used to record FESEM (field-emission scanning electron microscope) images. Imaging of surface topography by NT-MDT, SOLVER, Nova-Tech was done. Particle size distribution and zeta potential scattering properties were performed by Malvern Zs90.

2.2. Synthesis of SiO_2 nanostructures

Silica nanostructures have been synthesized by two methods: sol-gel and hydrothermal. Cell silica nanostructures are prepared by the Stober method, which is a subset of the sol-gel process.

2.2.1. Sol-gel

In this method, four substances are used to prepare for tuberculosis. First, distilled water, which acts as a hydrolyzer, is mixed with ethanol (solvent) for 5 minutes. Then add 2 ml of TEOS to the solution and stir for 5 minutes. Ammonia was used as the base catalyst for the synthesis of nanoparticles by adding ammonia dropwise to the solution to change the color of the solution from clear to white, then stirring the solution for 30 minutes. All steps are performed at room temperature.

2.2.2. Hydrothermal

Once the cell has been made, it is transferred to an autoclave and placed in an oven at 70° C for 4 hours to perform the compaction process at constant pressure and temperature. Then the aging time for tuberculosis is considered for 7 days before covering.

2.2.3. Coating of silica nanoparticles and heat treatment

There are various methods for creating a super-water-repellent coating on the glass surface, such as immersion coating, rotating coating, and spraying. The rotational coating was chosen to create a uniform, nanometer coating, with the glass slide on the turntable and a vacuum pump used to hold the glass in place at the time. It is then poured on the side of the glass using a 0.5 ml syringe of silica cell. The turntable then rotates at 2000 rpm for 20 seconds. The glass slide is then placed in the oven at 100 degrees for 3 hours.

2.2.4. Surface modification and heat treatment

The glass slide is then placed on the turntable according to the coating. PDMS has been used as an agent to modify silica nanoparticles and ultra-hydrophobic glass surfaces. After correcting the surface, the aging time is considered for 7 days. The glass was then placed in a furnace at 400° C for 3 h. At the end of the sample, the necessary tests were performed to check the properties

3. Results And Discussion

3.1. Design-Expert and analysis of results

There are two factors for making a super-waterproof coating: rough surface and rough surface correction. The StÖber method is one of the methods for synthesizing silica nanoparticles to make a rough surface. The purpose of designing the experiment is to optimize the parameters of the StÖber method to create a suitable rough surface and a surface modifying agent for the superhydrophobic coating. Finally, TEOS was investigated as a fixed precursor and the effect of deionized water (A), ethanol (B), ammonia (C), and PDMS (D). The central composite design (CCD) method was used for the design.

In this method, the experimental design is performed by specifying the actual levels and coding levels for each parameter (ie for high levels + 1, central levels zero, and low levels − 1). Actual and coded levels are shown in Table 1. The experimental design matrix with the levels encoded by the software is shown in Table 2. The obtained contact angle was entered into the software as a response.

Table 1
Actual levels and coded reaction parameters

Factors	Code and Level		
	-1	00	+1
A: Distilled water	8	10	12
B: Ethanol	10	12	14
C: Ammonia	6	9	12
D: Polydimethylsiloxane	20	30	40

Table 2
Experimental design matrix with coded surfaces

RUN	Factors				WCA Actual
	A	B	C	D	
1	0	-2	0	0	125.7
2	-1	1	-1	-1	119.2
3	-1	1	1	-1	132.9
4	-1	-1	1	1	142.4
5	2	0	0	0	130.7
6	0	0	0	0	166.5
7	0	0	0	0	165.5
8	-1	1	-1	1	112.7
9	-1	-1	-1	-1	117.3
10	-1	1	1	1	110.4
11	-2	0	0	0	118.5
12	0	0	0	0	164.5
13	0	0	0	0	165.8
14	0	2	0	0	121.5
15	1	1	1	1	125.8
16	0	0	0	-2	137.9
17	-1	-1	1	-1	136.2
18	1	1	-1	1	139.7
19	1	1	1	-1	146.1
20	1	-1	-1	1	145.1
21	0	0	0	0	166.3
22	0	0	2	0	132.8
23	1	-1	-1	-1	112.4
24	0	0	0	2	142.4
25	0	0	0	0	165.5

RUN	Factors				WCA Actual
26	1	-1	1	-1	121.3
27	1	-1	1	1	132.3
28	1	1	-1	-1	141.4
29	0	0	-2	0	127.1
30	-1	-1	-1	1	146.8

3.1.1 ANOVA analysis

According to the obtained statistical data and the ANOVA table, it is a good model that has the following two conditions:

1- p-value < 0/05

2- In the selected model, R^2 should be closer to one (Table 3).

Table 3
Quality of fitted to experimental data

R^2	**0.9980**
Adjusted R^2	0.961
Predicted R^2	0.9895
Adeq Precision	71.9315

R^2 checks the quality of the experimental data with the model and the best value is one.

Adj- R^2 is the modified value of R^2, which also takes into account the degree of freedom (number of factors).

The projected RU of 0.9897 agrees with the adjusted RU of 0.9961; That is, the difference is less than 0.2.

The model measures the accuracy of the signal-to-noise ratio. A ratio greater than 4 is desirable. The obtained ratio shows 72,397 sufficient signals. This model can be used to move in the design space.

Statistical data were analyzed using the response level method and regression equation:

Regression equation in encrypted units

CA = 165.683 + 2.94208 * A + -1.41625 * B + 0.994583 * C + 1.55708 * D + 6.84688 * AB + -2.44063 * AC + 0.938125 * AD + -0.533125 * BC + -8.14938 * BD + -4.97438 * CD + – 10.1651 * A2 + -10.4151 * B2 + -8.83635 * C2 + -6.29135 * D2

The quadratic response level model is used to evaluate the effectiveness of the parameters and the accuracy of the model.

The value of model F / 664 indicates that the model is acceptable. There is only a 0.01% chance that an F value of this magnitude will occur due to the disturbance.

P values less than 0.0500 indicate that the model parameters are significant. In this case, A, B, C, D, AB, AC, AD, BD, CD, A^2, B^2, C^2, D^2 are acceptable parameters. Values greater than 0.000 indicate that the model conditions are not acceptable. If many model parameters are not acceptable, changing the model may improve your model.

Lack of Fit A value of 3.12 indicates that a mismatch to a pure error is not acceptable. There is an 11.08% chance that a mismatch of the F value of this magnitude will occur due to a disturbance. Insignificant disproportion is good because we want the model to fit Table 4.

Table 4
Analysis of variance

Source	Sum of Squares	df	Mean Square	F-value	p-value	
Model	9135.54	14	652.54	528.44	< 0.0001	significant
A-H_2O	207.68	1	207.68	168.19	< 0.0001	significant
B-EtOH	48.17	1	48.17	39.01	< 0.0001	significant
C-NH_3	24.40	1	24.40	19.76	0.0005	significant
D-PDMS	58.28	1	58.28	47.20	< 0.0001	significant
AB	748.02	1	748.02	605.77	< 0.0001	significant
AC	95.06	1	95.06	76.98	< 0.0001	significant
AD	14.06	1	14.06	11.39	0.0042	significant
BC	4.41	1	4.41	3.57	0.0783	
BD	1062.76	1	1062.76	860.65	< 0.0001	significant
CD	396.01	1	396.01	320.70	< 0.0001	significant
A^2	2842.02	1	2842.02	2301.54	< 0.0001	significant
B^2	2983.34	1	2983.34	2415.98	< 0.0001	significant
C^2	2144.23	1	2144.23	1736.45	< 0.0001	significant
D^2	1085.76	1	1085.76	879.28	< 0.0001	significant
Residual	18.52	15	1.23			
Lack of Fit	15.99	10	1.60	3.16	0.1078	not significant
Pure Error	2.53	5	0.5057			
Cor Total	9154.07	29				

3.1.2. Diagnostics diagrams

To troubleshoot the results obtained from the software the four graphs of normal probability, residuals vs. predicted, predicted vs. actual and Box-Cox plot for power transforms are used. In Fig. 1a, the normal probability diagram shows that the residuals follow a normal distribution, therefore they follow a straight line. Even with normal data, expect some scatter. Figure 1b (residuals vs. predicted) indicates that the residuals are bullish against the predicted response values. This plot tests the assumption of constant variance. The graph should have a random scatter and according to the graph the data follows a random scatter. Figure 1c shows predicted vs actual. A graph of the predicted response values versus the actual response values. The purpose is to detect a value, or group of values, that are not easily predicted by the

model. The Box-Cox chart is used to determine the strength of metamorphism consistent with experimental data (Fig. 1d). The blue line in the diagram shows the model change and the green line shows the best lambda value. The red line indicates the 95% confidence interval associated with the best amount of lambda. It is said that a model is qualified for the blue conversion line between the red lines and the green line on the conversion curve to form a black and white curve. The graph shows that the blue transition line between the green line and the red line shows that the model matches the experimental results.

3.1.3. Influence of single variables on contact angle

Figure 2 shows the effect of the selected parameters on the contact angle. The graph follows a certain pattern for all parameters. With increasing water concentration from 8 to 10, the contact angle gradually increased from 152.34 degrees to 165.83 degrees. Subsequently, with an increase from 10 to 12, the contact angle decreased from 165.83 degrees to 158.45 degrees. For the parameters of ethanol, ammonium hydroxide, and PDMS, the same changes occurred, ie the contact angle increased from − 1 to zero and decreased from zero to + 1.

3.1.4. The effect of binary variables on the contact angle

In Fig. 3, the interaction and three-dimensional diagrams of the model are obtained to estimate the interaction between the variables and the contact angle, while the other variables are kept at their zero levels and the others change in the experimental range. In Fig. 3, as can be seen, the interaction of the binary parameters with each other is like the effect of the parameters individually. The difference between the interaction of the binary parameters with each other is in the angle between the two diagrams. The higher the angle of the two graphs, the greater the interaction, and if they are parallel, they have less or no interaction. According to the ANOVA table, the BC parameter is unacceptable, and the BC.

3.1.5. Process design optimization

One of the purposes of test design is to optimize process parameters to obtain the highest contact angle. The size of the contact angle was determined to be 162 degrees. According to the CCD design, the optimal conditions for the preparation of SiO_2 sol are shown in Fig. 4. The experimental contact angle size for the optimized sample is compared with the predicted contact angle in Fig. 4. The results showed that the size of the experimental contact angle corresponds well with the predicted contact angle and shows that the CCD surface response surface method is an efficient method for preparing ultra-waterproof coatings with a contact angle above 160°.

3.2. Identify the optimized sample

Optimized sample according to statistical data analysis, as mentioned earlier, was prepared by Stober method with TEOS as precursor, deionized water of hydrolyzing agent, solvent ethanol, ammonium

hydroxide catalyst, and PDMS as a hydrophobic agent. As a result, the effect of experimental parameters on superhydrophobic coatings was investigated.

3.2.1 Optimized sample contact angle

The contact angle is the angle between the surface on which the liquid is located or the point of connection of the liquid on the surface. Static and dynamic contact angles are of its types. The method of measuring the contact angle is called the baseless droplet method. Can be used. The contact angle obtained for the optimized sample is 162 degrees (Fig. 5).

3.2.2. XRD studies

Figure 6 shows the X-ray diffraction pattern of nanoparticles prepared by the Stuber method. As shown in the figure, no diffraction peaks are observed except for broadband with a 24-degree center (JCPDS No. 0085 – 29) which represents a completely amorphous structure. But using Highscore plus software, it is shown that a small part of the sample has a crystalline structure. The marked peaks are related to hexagonal (JCPDS number 2147-080-01) and quadrilateral (JCPDS number 0430-079-01) and (JCPDS number 0513-082-01) crystal structures.

3.2.3. FTIR spectrum

Infrared spectroscopy (FT-IR) was performed at room temperature to investigate the chemical bonds created in the optimized sample. As shown in Fig. 7, the peaks of 3440 cm^{-1} and 1624 cm^{-1} are symmetrical tensile vibration and flexural vibration of the O-H bond, respectively, due to the incomplete density of the silanol group. The range of 400 $cm^{-1}$to 1350 cm^{-1}, known as the fingerprint area, indicates silicon bonds. The peak 1095 cm^{-1} and 808 cm^{-1} represent the symmetric and asymmetric tensile vibrations of the Si-O-Si bond and the peak 466 cm^{-1} represents the flexural vibrations of the Si-O-Si. The peak of 947 $cm^{-1}$is due to the flexural vibrations of the Si-OH bond [31, 32].

3.2.4. SEM images

Scanning electron microscope images of the optimized sample at different magnifications are shown in Fig. 8. As seen in Fig. 8a, the nanostructures have spherical morphology with uniform size distribution. Particle size using image j software is approximately 250 nm. The reason for the growth of nanoparticles is due to the use of the hydrothermal method to create a suitable uneven surface on the glass surface.

Figures 8b and 8c show the scanning electron microscope image of the surface and cross-section. The roughness of the glass surface indicates a rough surface for the super-hydrophobic coating. The growth process of this superhydrophobic coating is island-layer, which is a state between layer-by-layer growth and island growth, one or more monolayers are formed and then the islands are completed. Another name for this growth process is Stransky-Kristanov. In this growth mode, a mismatched network may be

formed between the coated layer and the substrate. The grain size of the thin layer that is formed on the substrate depends on the speed and temperature of the layer. The thickness of this superhydrophobic coating is reported to be 1.06 µm.

3.2.5. EDS studies

Figure 9a shows the X-ray energy diffraction spectrum for the optimal sample. As shown in the figure, the purely synthesized optimized sample is composed of silicon and oxygen elements. Figure 9b shows the X-ray diffraction spectrum from the glass surface. Due to the use of PDMS as a hydrophobic agent on the glass surface, in addition to silicon and oxygen, carbon is also seen. The gold peak seen in the figure is due to the conductivity of the surface for SEM analysis.

3.2.6. AFM images

Atomic force microscopy images of the mean square root roughness for the optimized sample are estimated in Fig. 10. As can be seen in the figure, rough surface roughness is created on the glass surface to create a super-hydrophobic coating. The maximum and minimum of these surface roughnesses were measured at 2.6 and 1.2 µm, respectively. The root means square roughness for the sample optimized by Gwyddion software was calculated to be 0.121 µm.

3.2.7. DLS analysis

As can be seen in the SEM images, the optimized sample has the same particle size distribution and DLS analysis was performed to determine the particle size distribution range. The particle size range is between 255 and 396.1 nm and, as shown in Fig. 11, the particle size distribution diagram is very narrow. The average particle size is 291.456 nm.

3.2.8. Chemical resistance test

The stability of superhydrophobic coating was investigated in three media: acidic, neutral, and alkaline. Figure 12 shows the effect of different environments on the contact angle. The superhydrophobic coating was immersed in 10 ml for 24 hours. It was then dried at room temperature. As can be seen in the figure, the play environment (pH: 13.5) has a great impact on the coating so that the drop contact angle of the super-hydrophobic range reaches the boundary between hydrophobic and hydrophilic, in which case the result can be the game environment causes corrosion of the coating and the use of this coating in play environments is not recommended. The contact angle obtained from the acidic environment (pH: 1) indicates that the coating has good resistance and this feature can be very effective in coating against acid rain. The use of deionized water is used to accurately assess the strength of the coating when in contact with water. Therefore, to prevent the effect of temperature on the coating, this test was performed at a temperature of 25 degrees. The contact angle resulting from the immersion of the coating in deionized water indicates the very good resistance of the coating in this environment.

4. Conclusions

- The test design was used to provide a superhydrophobic coating to optimize the test conditions to save time and money and obtain the best answer for the test parameters.
- The central composite design method was used to perform all possible experiments to obtain the best result.
- Silica nanostructures were synthesized by the sol-gel-hydrothermal method according to the number of experiments and designed values and the rotational coating was used to create a thin layer on the glass.
- The contact angle of each experiment was examined as the answer by the software and the optimized values of the experimental parameters were used to synthesize the optimized sample.
- The optimized sample was identified by the relevant analyzes and the following results were obtained:

1- To prove the superhydrophobic coating, the contact angle between the drop and water was examined and an angle of 162 degrees was obtained.

2- The powder obtained from silica cells was examined and according to XRD analysis, it is a large part of the amorphous nanostructure. And according to the FT-IR spectrum, the Si-O-Si bond was detected.

3- Silica nanostructures have a uniform spherical morphology with a particle size between 255–396 nm and the thickness of this nanostructure is 1.06 μm. The surface roughness on the glass surface indicates a super-hydrophobic coating.

4- According to SEM images and DLS analysis, the optimized sample has a uniform size distribution and according to the amount of zeta potential obtained, it has a desirable dispersion property.

5- For chemical resistance, the coating was placed in three environments of acidic, neutral, and alkaline for 24 hours, and according to the contact angle obtained, it can be concluded that the coating ¬supplied hydrophobic in neutral environments ¬ It is more than in other environments.

Declarations

Acknowledgment

This work was supported by the University of Semnan and the author thanks for this assistance.

Data availability

The datasets used and analyzed during the current study available from the corresponding author on reasonablerequest.

References

1. Ulaeto, S.B., Rajan, R., Pancrecious, J.K., Rajan, T. & Pai, B. Developments in smart anticorrosive coatings with multifunctional characteristics. *Prog. Org. Coat*. **111**, 294-314 (2017).
2. Wei, H. *et al.* Advanced micro/nanocapsules for self-healing smart anticorrosion coatings. *J. Mater. Chem*. A. **3**, 469-80 (2015).
3. Makhlouf, A. Protective coatings for automotive, aerospace and military applications: current prospects and future trends. Handbook of Smart Coatings for Materials Protection: Elsevier; (2014) 121-131.
4. Chisholm, B.J., Christianson, D.A., Stafslien, S.J., Gallagher-Lein, C. & Daniels, J. Novel, environmentally friendly, antifouling/fouling release coatings developed using combinatorial methods. ACS Publications. 127-141 (2009).
5. Challene, C. Smart Coatings: Reaching the Big Time with Many More Opportunities. *JCT COATINGSTECH*. **14**, 22-27 (2017).
6. Montemor, M.D.F. Functional and smart coatings for corrosion protection: A review of recent advances. *Surf. Coat. Technol.***258**, 17-37 (2014).
7. Hosseini, M. & Makhlouf, A.S.H. Industrial applications for intelligent polymers and coatings. Springer. (2016).
8. Cole, I. Smart coatings for corrosion protection: an overview. Handbook of Smart Coatings for Materials Protection. **29**, 29-55 (2014).
9. Carneiro, J., Teixeira, V. & Azevedo, S. Smart self-cleaning coatings for corrosion protection. Handbook of Smart Coatings for Materials Protection: Elsevier. 489-509 (2014).
10. Ulaeto, S.B., Pancrecious, J.K., Rajan, T. & Pai, B. Smart Coatings. Noble Metal-Metal Oxide Hybrid Nanoparticles: Elsevier. 341-372 (2019).
11. Rtimi, S., Sanjines, R., Pulgarin, C. & Kiwi, J. Quasi-instantaneous bacterial inactivation on Cu–ag nanoparticulate 3D catheters in the dark and under light: mechanism and dynamics. *ACS Appl. Mater. Interfaces*. **8**, 47-55 (2016).
12. Rtimi, S., Giannakis, S. & Pulgarin, C. Self-sterilizing sputtered films for applications in hospital facilities. *Molecules*. **22**, 1074 (2017).
13. Guin, A.K., Nayak, S., Bhadu, M.K., Singh, V. & Rout, T.K. Development and performance evaluation of corrosion resistance self-healing coating. *Int. Scholarly Res*. (2014).
14. Abdollahi, H., Ershad-Langroudi, A., Salimi, A. & Rahimi, A. Anticorrosive coatings prepared using epoxy–silica hybrid nanocomposite materials. *Indust. Eng. Chem. Res*. **53**, 10858-10869 (2014).
15. Guldin, S. *et al.* Self-cleaning anti-reflective optical coatings. *Nano Lett*. **13**, 5329-5335 (2013).
16. Stieberova, B. *et al.* Application of ZnO nanoparticles in a self-cleaning coating on a metal panel: an assessment of environmental benefits. *ACS Sustainable Chem. Eng*. **5**, 2493-2500 (2017).

17. Das, S., Kumar, S., Samal, S.K., Mohanty, S. & Nayak, S.K. A review on superhydrophobic polymer nanocoatings: recent development and applications. *Ind. Eng. Chem. Res*. **57**, 2727-2745 (2018).
18. England, M.W., Urata, C., Dunderdale, G.J. & Hozumi, A. Anti-fogging/self-healing properties of clay-containing transparent nanocomposite thin films. *ACS Appl. Mater. Interfaces.***8**, 4318-4322 (2016).
19. Zhang, B., Zhao, X., Li, Y. & Hou, B. Fabrication of durable anti-corrosion superhydrophobic surfaces on aluminum substrates via a facile one-step electrodeposition approach. *RSC Adv*. **42**, 35455-35465 (2016).
20. Cai, Z., Lin, J. & Hong, X. Transparent superhydrophobic hollow films (TSHFs) with superior thermal stability and moisture resistance. *RSC Adv*. **8**, 491-498 (2018).
21. Syed, J.A., Tang, S. & Meng, X. Super-hydrophobic multilayer coatings with layer number tuned swapping in surface wettability and redox catalytic anti-corrosion application. *Sci. Rep*. **7**, 1-17 (2017).
22. Yuan, J., Wang, J., Zhang, K. & Hu, W. Fabrication and properties of a superhydrophobic film on an electroless plated magnesium alloy. *RSC Adv*. **7**, 28909-28917 (2017).
23. Zhang, X. *et al.* A one-pot sol-gel process to prepare a superhydrophobic and environment-resistant thin film from ORMOSIL nanoparticles. *RSC Adv*. **4**, 9838-9841 (2014).
24. Hench, L.L. & West, J.K. The sol-gel process. *chem. Rev*. **90**, 33-72 (1990).
25. Oben, D.T. Synthesis of Advanced Hybrid Polymeric Nanomaterials and Characterization of Novel Silsesquioxanes with Desirable Superhydrophobic Coating Properties: The Open University. (2016).
26. Wu, Y. *et al.* Facile spraying fabrication of highly flexible and mechanically robust superhydrophobic F-SiO_2@ PDMS coatings for self-cleaning and drag-reduction applications. *New J. Chem*. **42**, 18208-18216 (2018).
27. Bahgat Radwan, A., Abdullah, A.M., Mohamed, A.M. & Al-Maadeed, M.A. New electrospun polystyrene/Al_2O_3 nanocomposite superhydrophobic coatings; synthesis, characterization, and application. *Coatings*. **8**, 65 (2018).
28. Jain, R. & Pitchumani, R. Facile fabrication of durable copper-based superhydrophobic surfaces via electrodeposition. *Langmuir*. **34**, 3159-3169 (2017).
29. Zhao, S. *et al.* Sequentially reinforced additive coating for transparent and durable superhydrophobic glass. *Langmuir*. **34**, 11316-11324 (2018).
30. Gu, H., Zhang, Q., Gu, J., Li, N. & Xiong, J. Facile preparation of superhydrophobic silica nanoparticles by hydrothermal-assisted sol-gel process and effects of hydrothermal time on surface modification. *J. Sol-Gel Sci. Technol*. **8**, 478-485 (2018).
31. Tran, T.N., Pham, T.V.A., Le, M.L.P. & Nguyen, T.P.T. Synthesis of amorphous silica and sulfonic acid functionalized silica used as a reinforced phase for polymer electrolyte membrane. *Adv. Nat. Sci.: Nanosci. Nanotechnol*. **4**, 45007 (2013).
32. Ramalla, I., Gupta, R.K. & Bansal, K. Effect on superhydrophobic surfaces on electrical porcelain insulator, improved technique at polluted areas for longer life and reliability. *Int. J. Eng. Technol*. **4**,

509 (2015).
33. Cheng, Y., Miao, D., Kong, L., Jiang, J. & Guo, Z. Preparation and performance test of the super-hydrophobic polyurethane coating based on waste cooking oil. *Coatings*. **9**, 861 (2019).

Scheme

Scheme 1 is available in supplementary section.

Figures

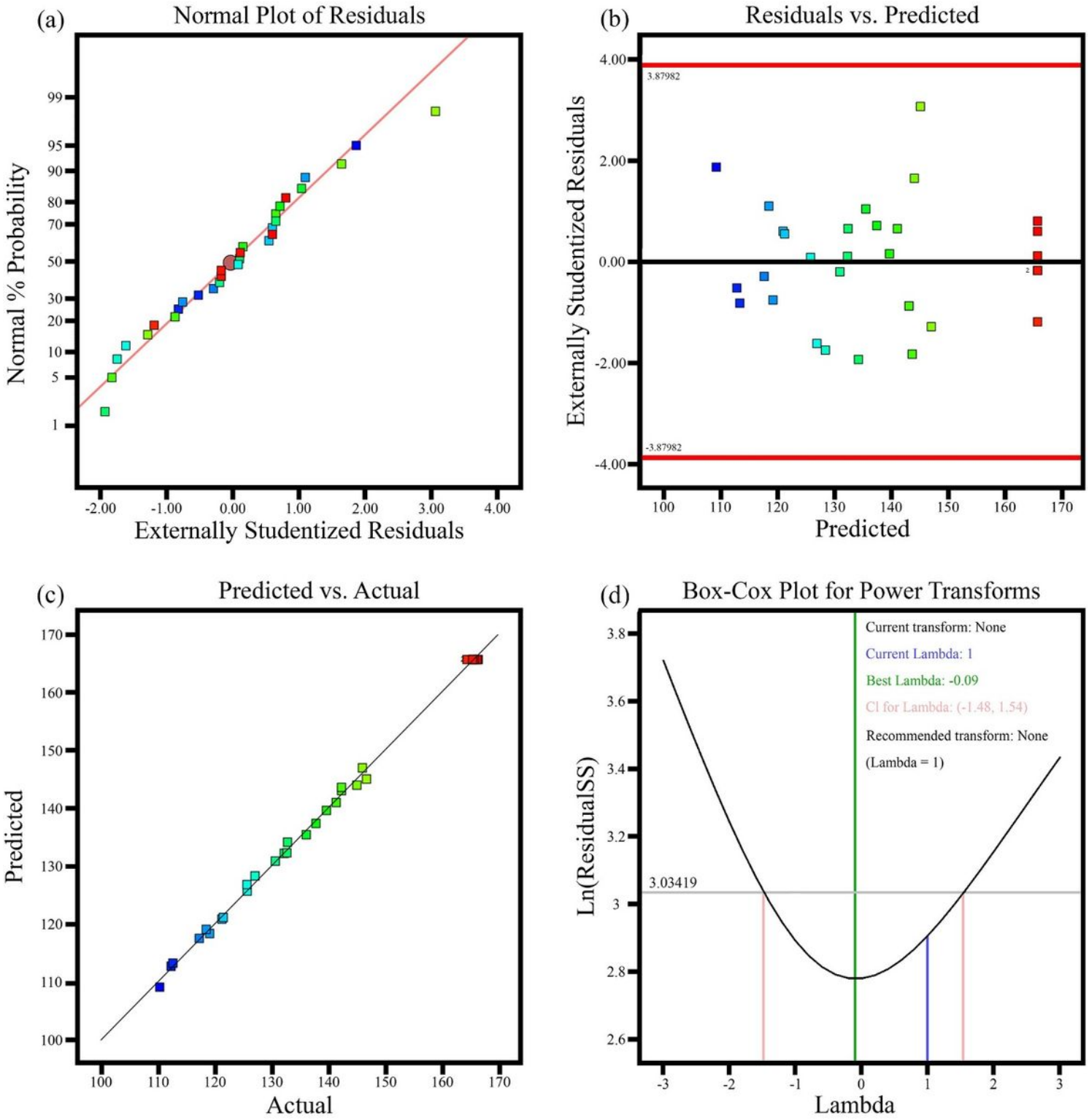

Figure 1

Diagnostics diagrams (a) **normal probability, (b) residuals vs. predicted, (c) predicted vs. actual and (d) Box-Cox plot for power transforms**

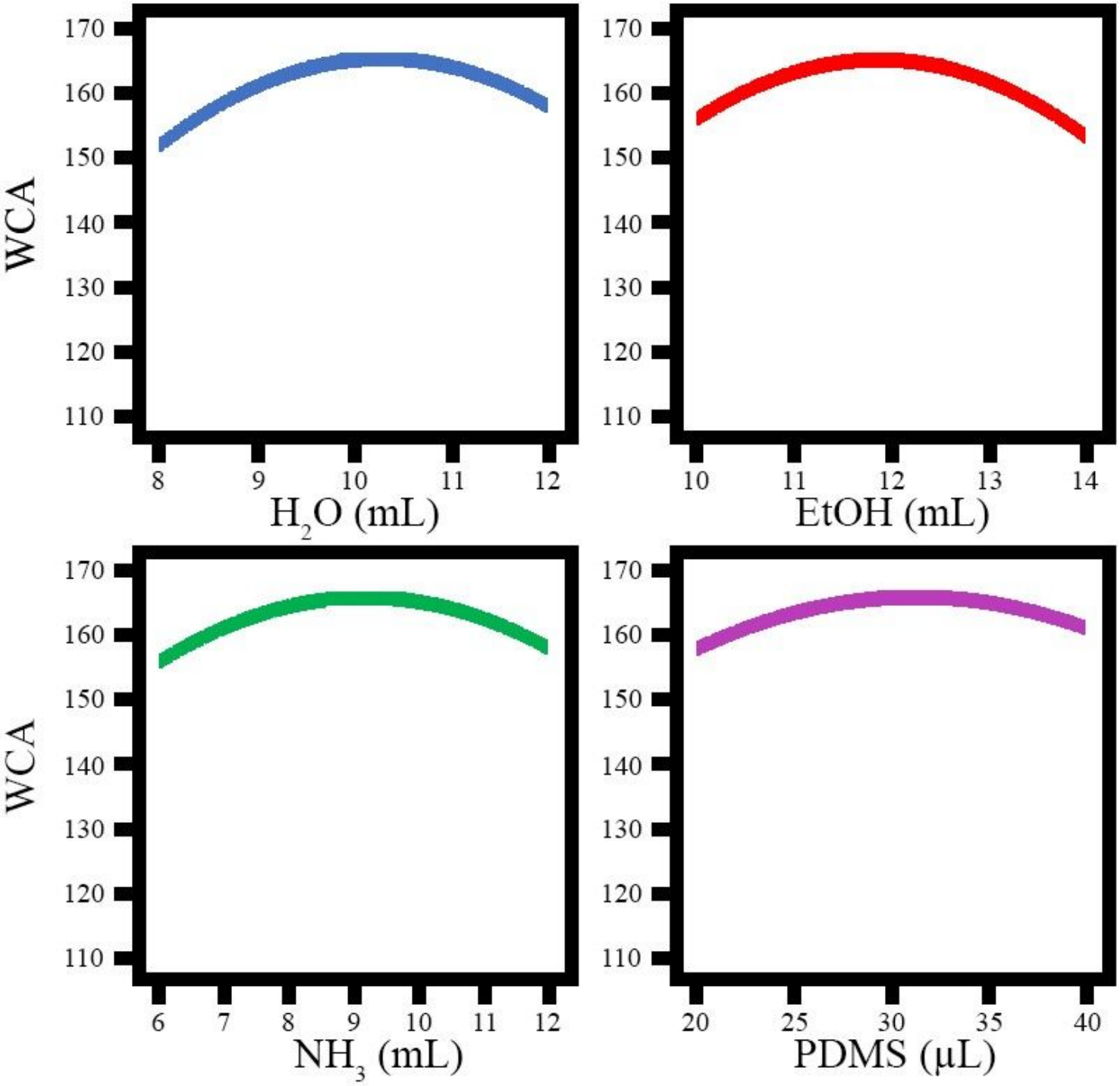

Figure 2

Influence of single variables on contact angle

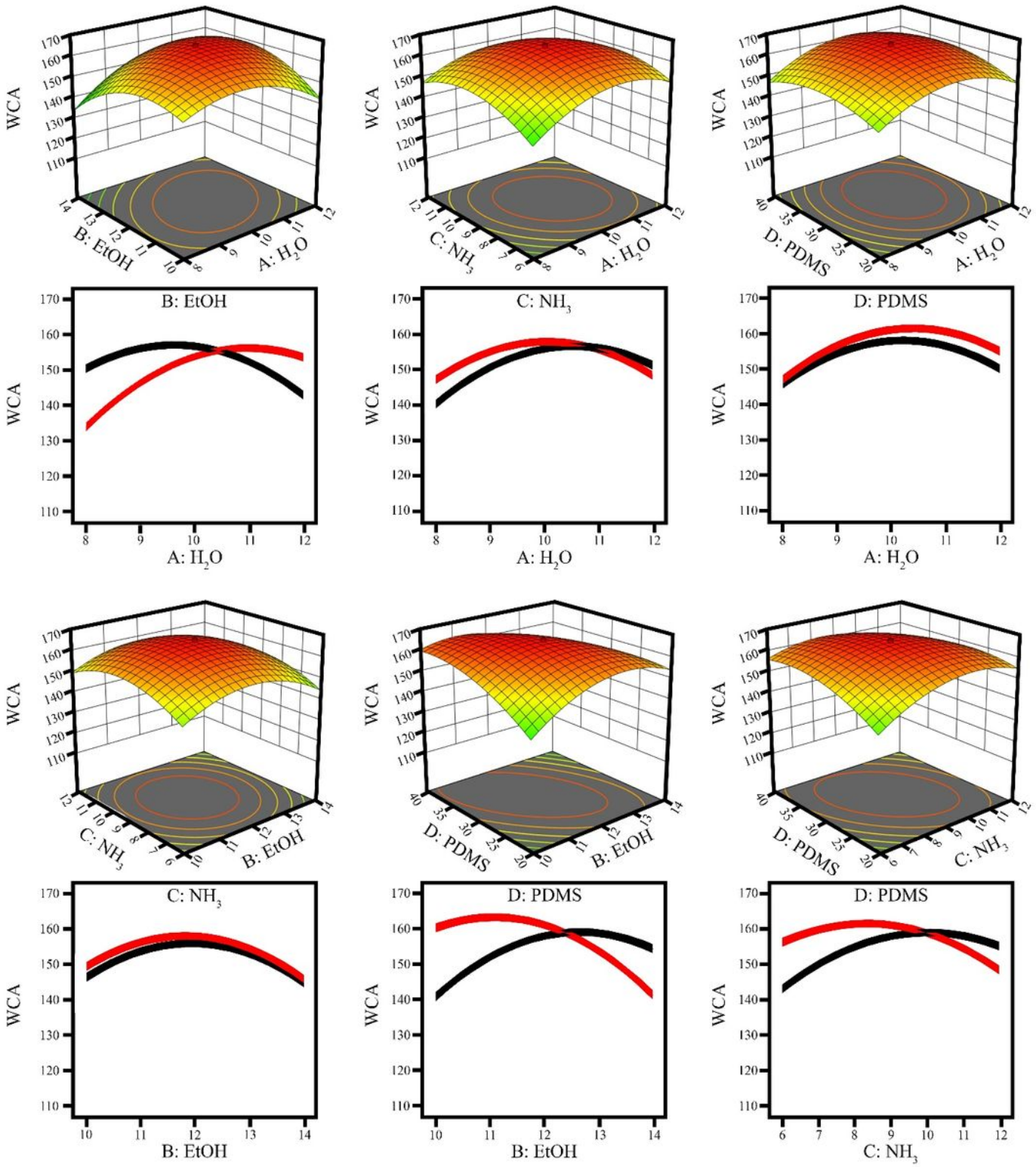

Figure 3

The effect of binary variables on the contact angle

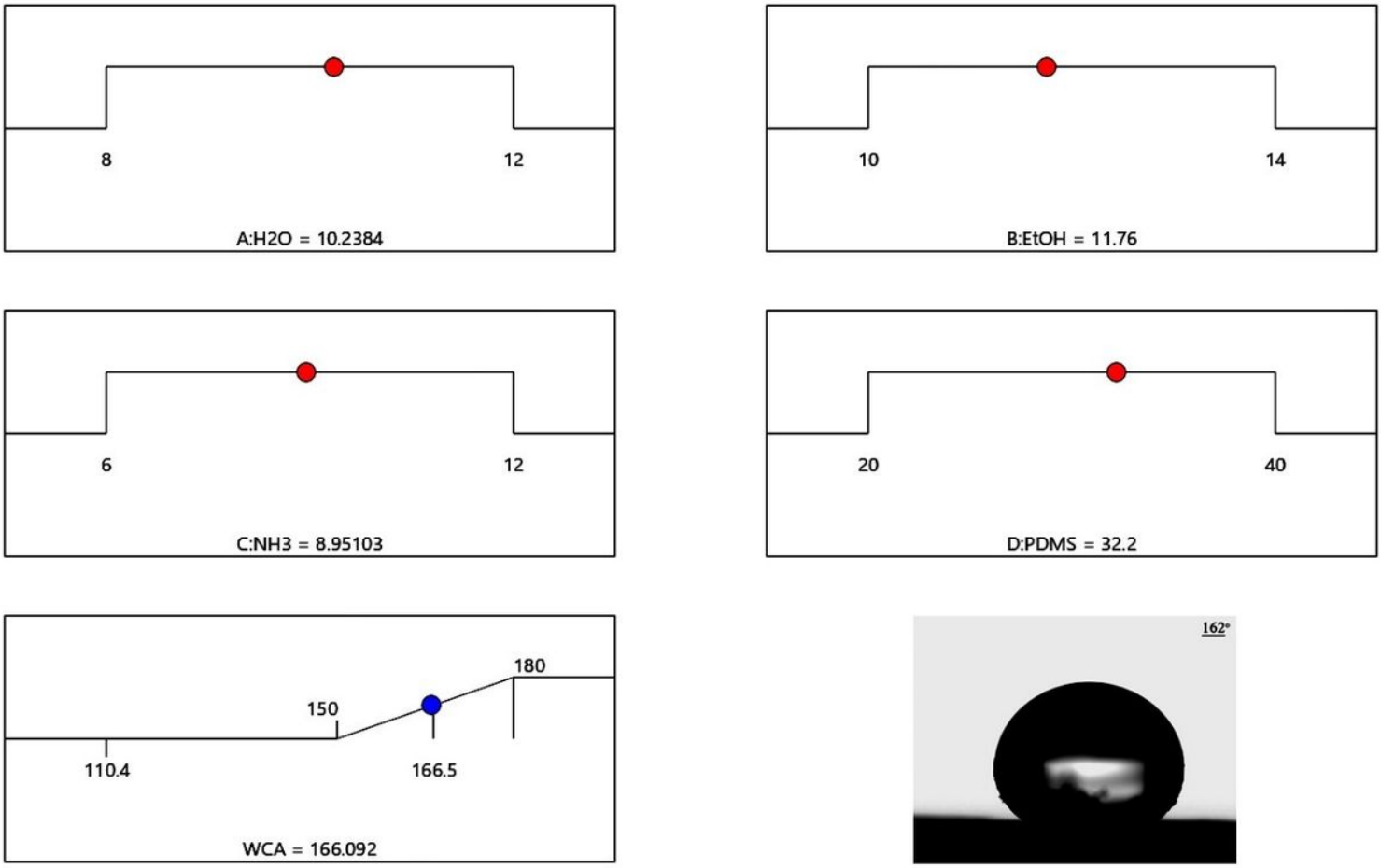

Figure 4

Optimal values of process parameters

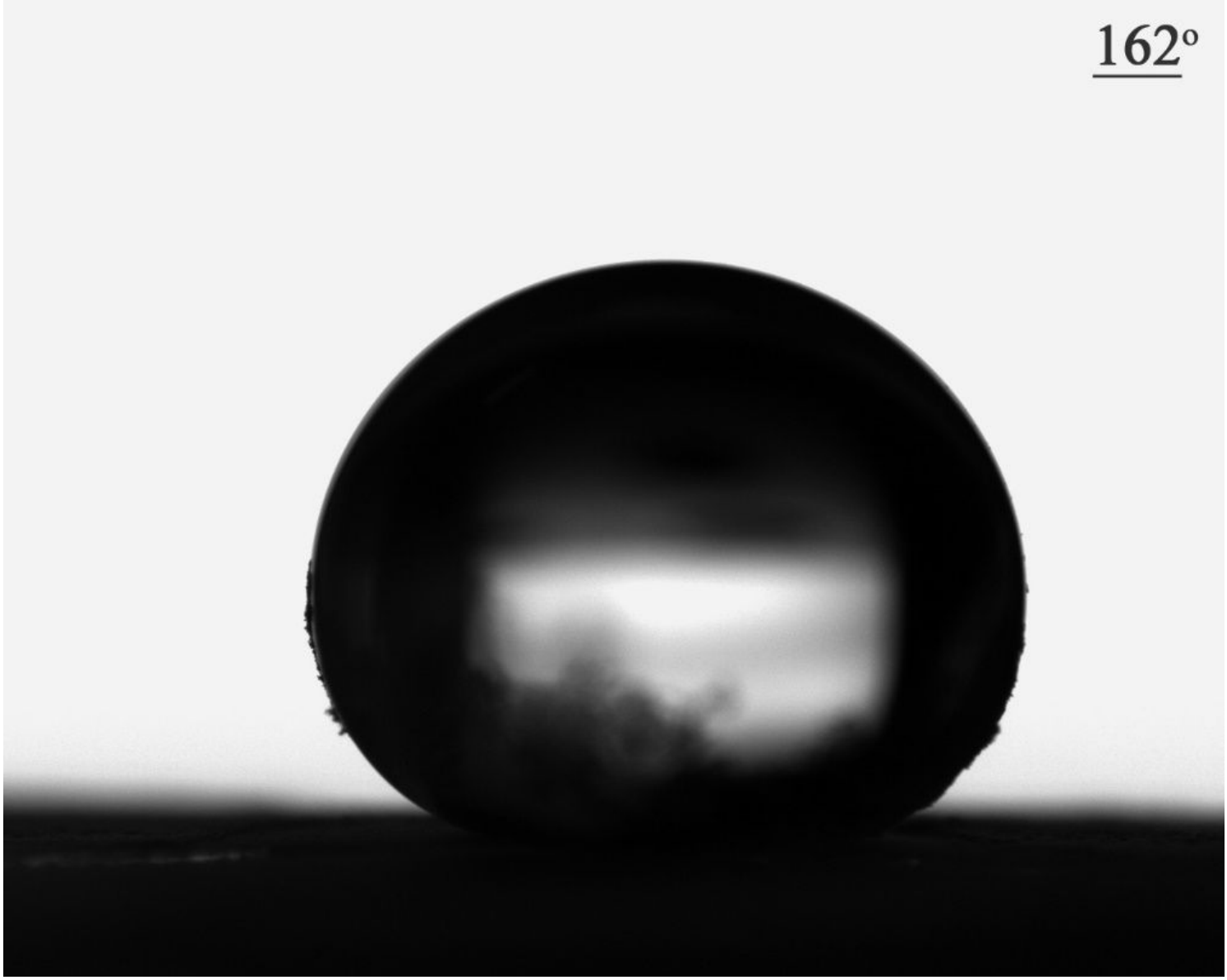

Figure 5

Contact angle between the drop and the glass surface

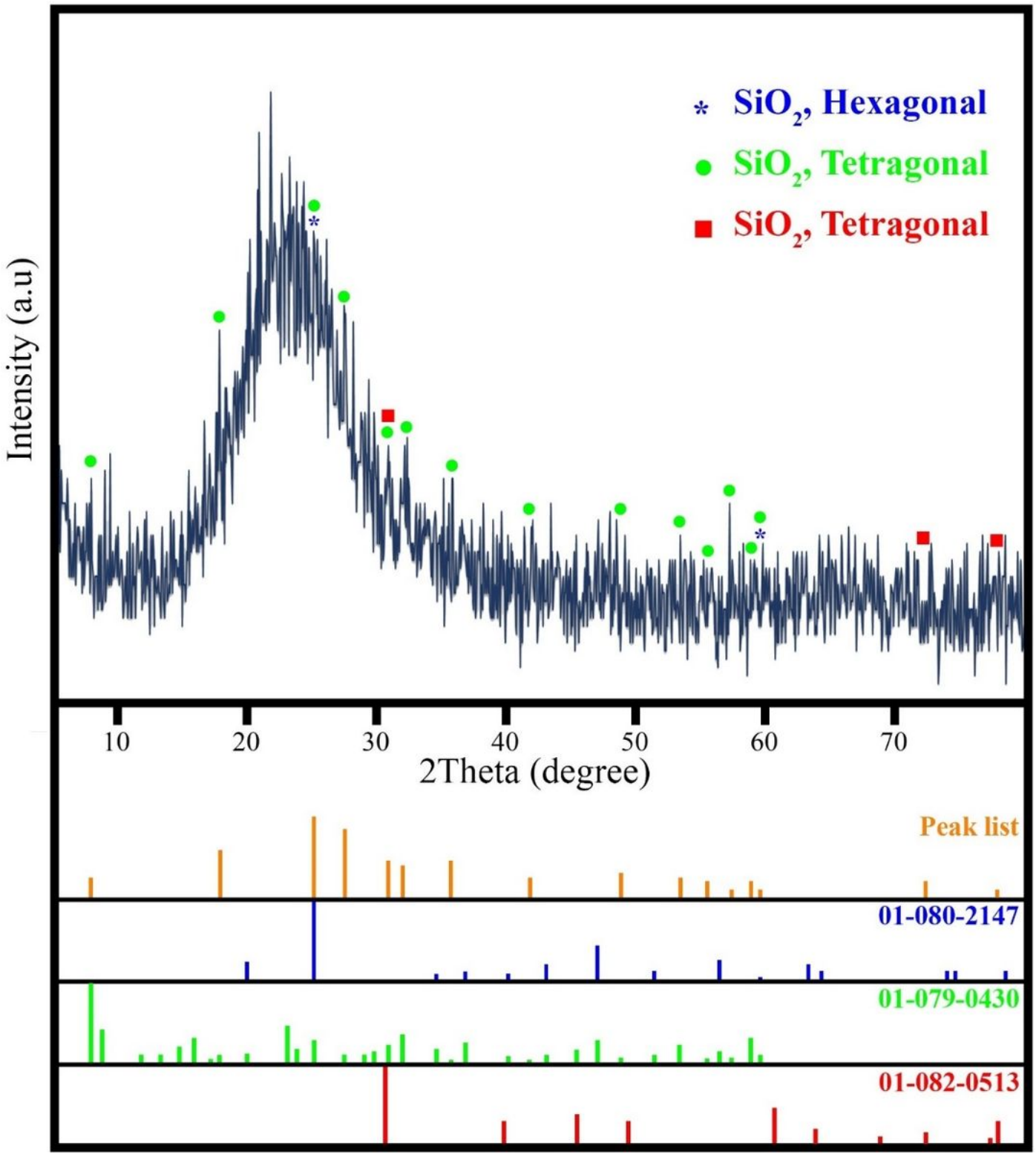

Figure 6

XRD pattern of the optimized sample

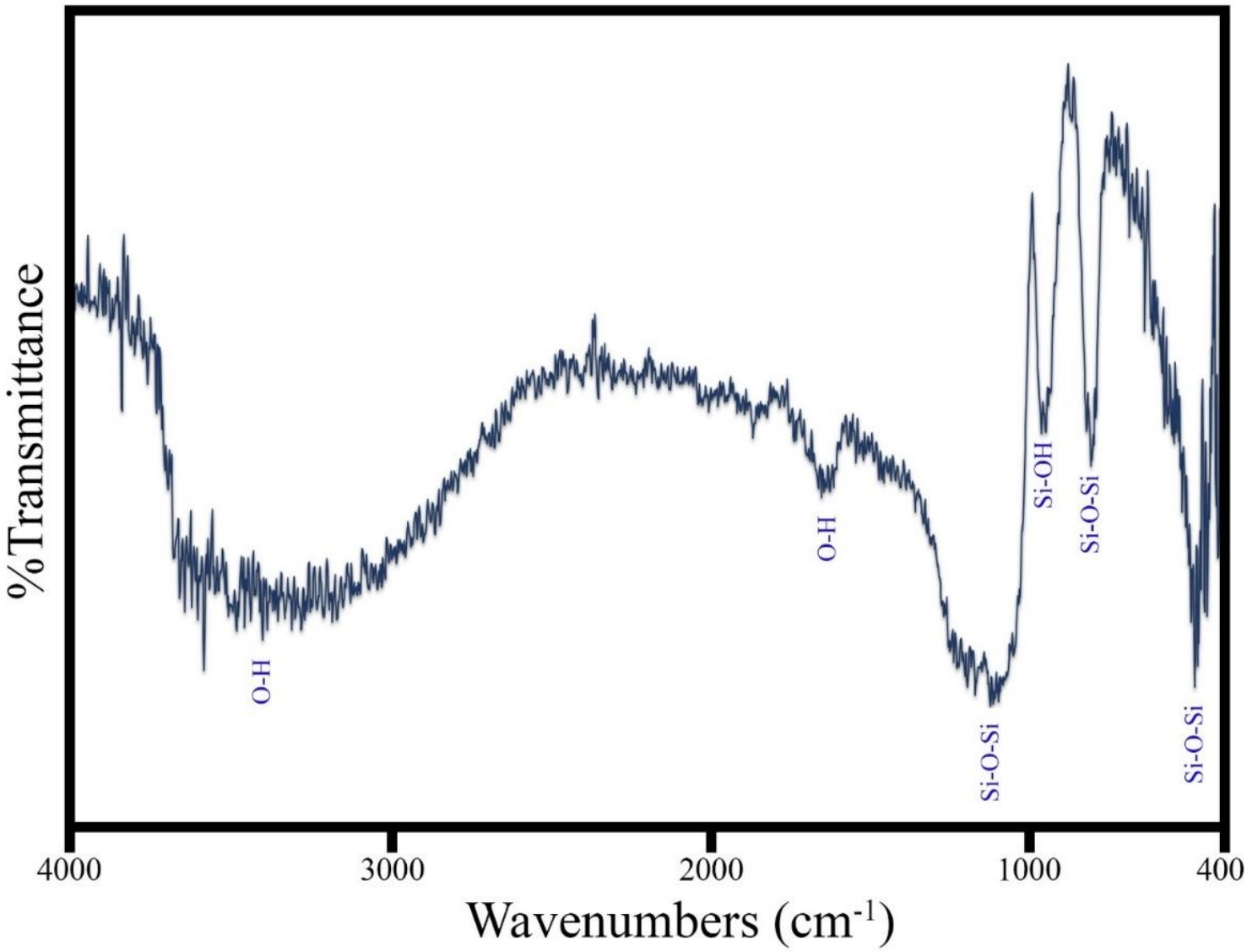

Figure 7

FT-IR spectrum of the optimized sample

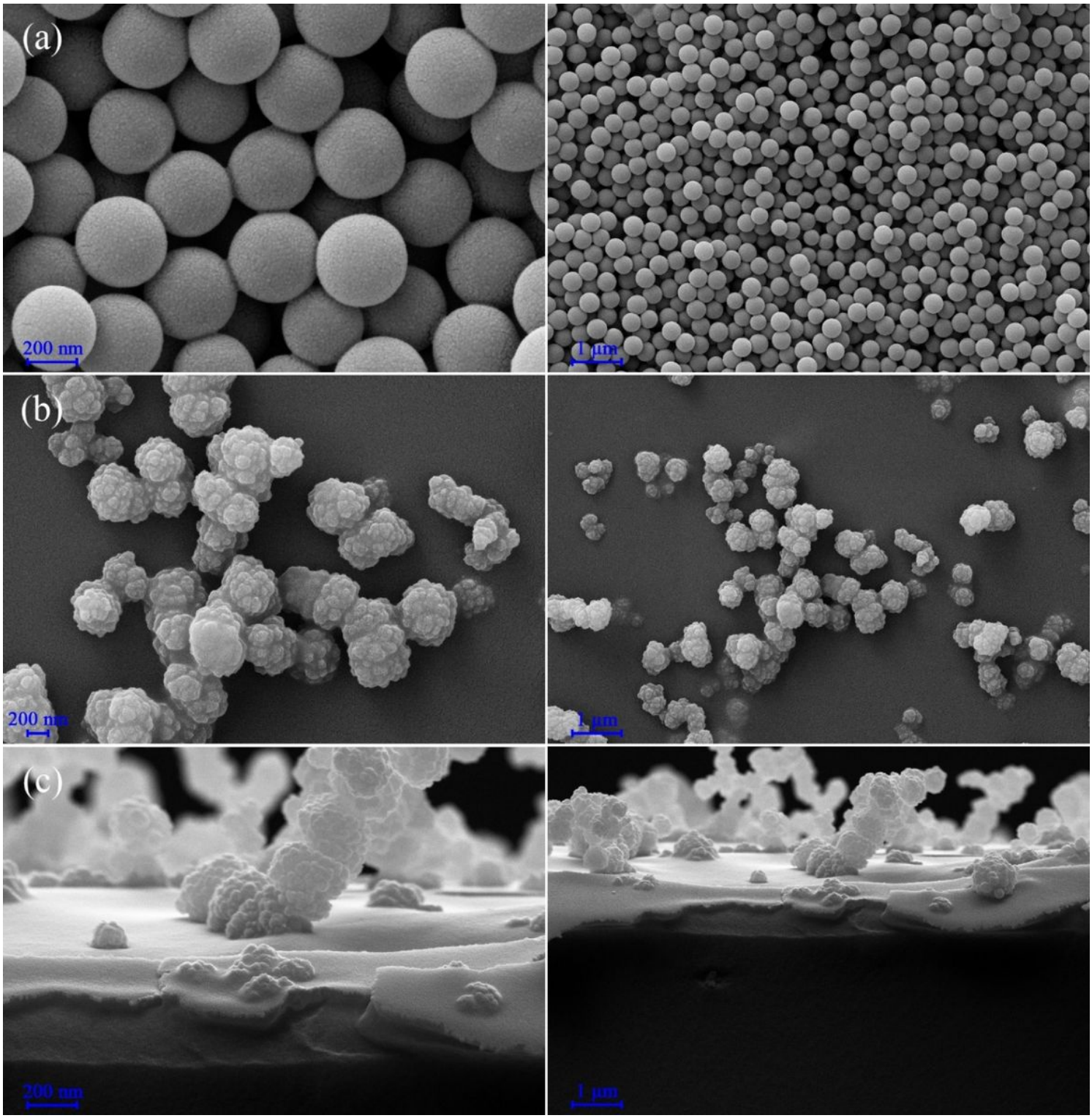

Figure 8

SEM images (a) the sample and (b) the glass surface and cross-section

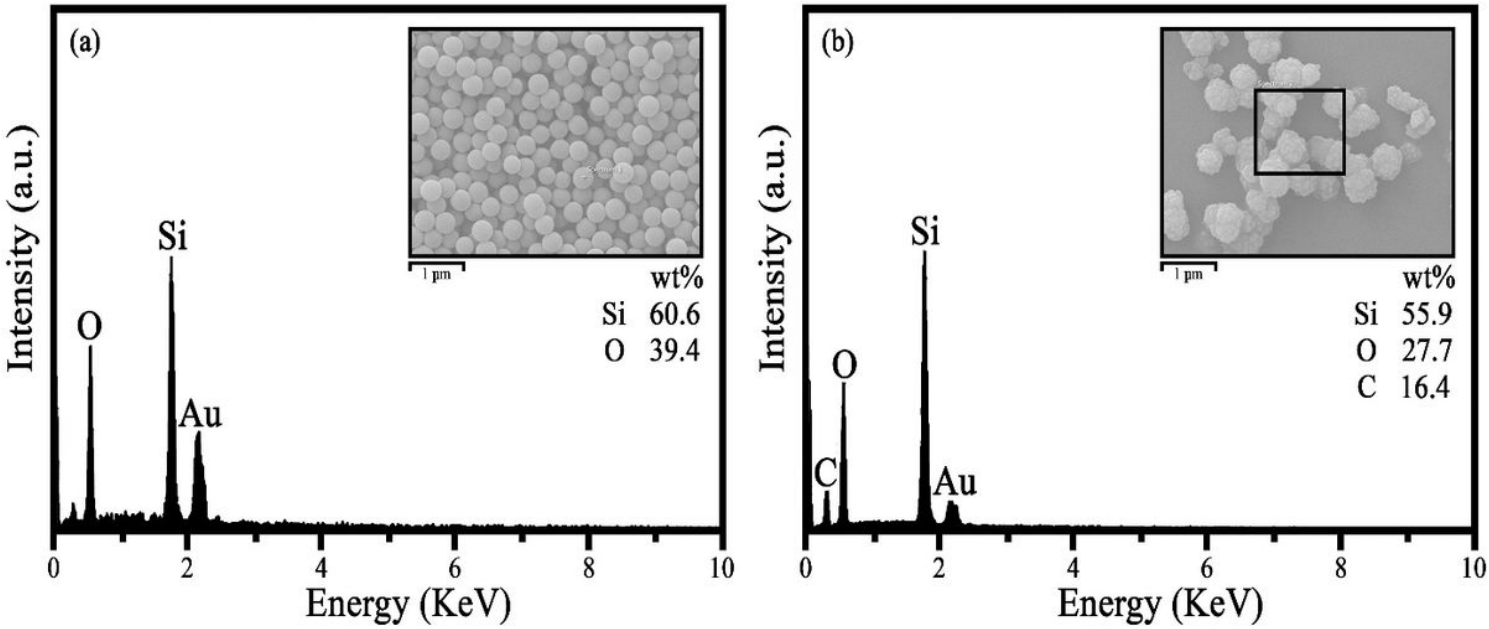

Figure 9

EDS for the optimized sample and the glass surface

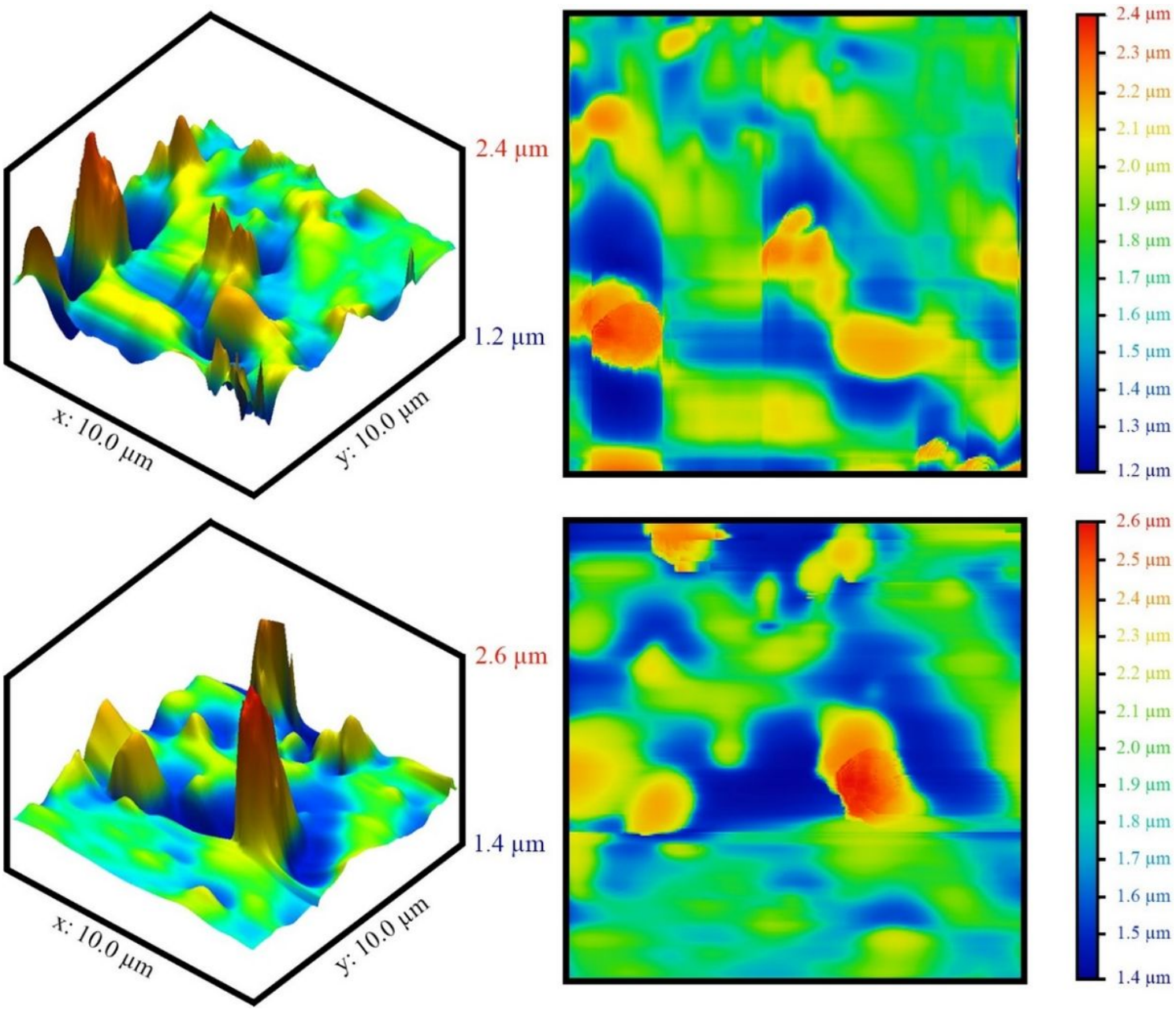

Figure 10

AFM images of the optimized sample

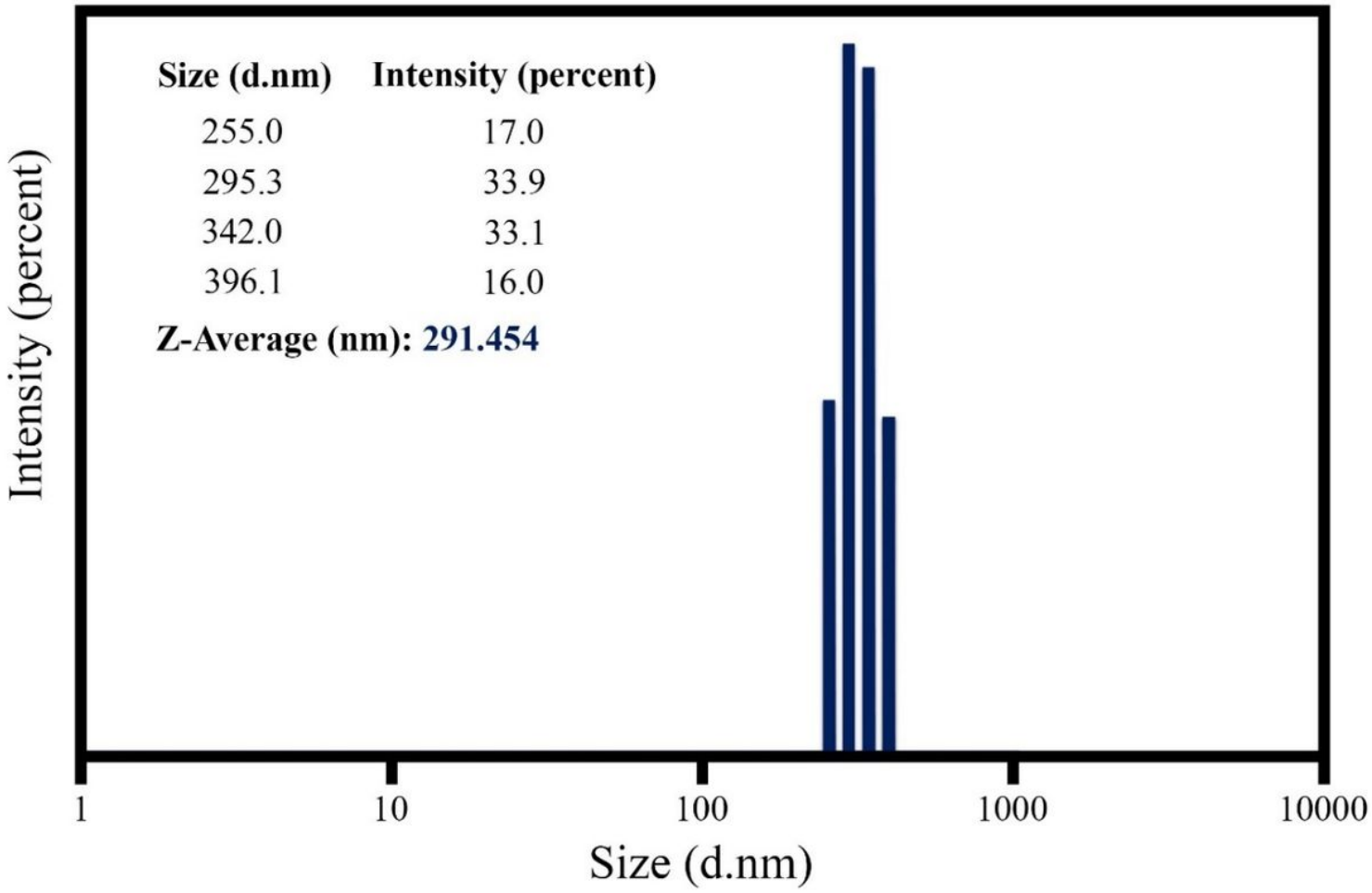

Figure 11

Size distribution of the optimized sample

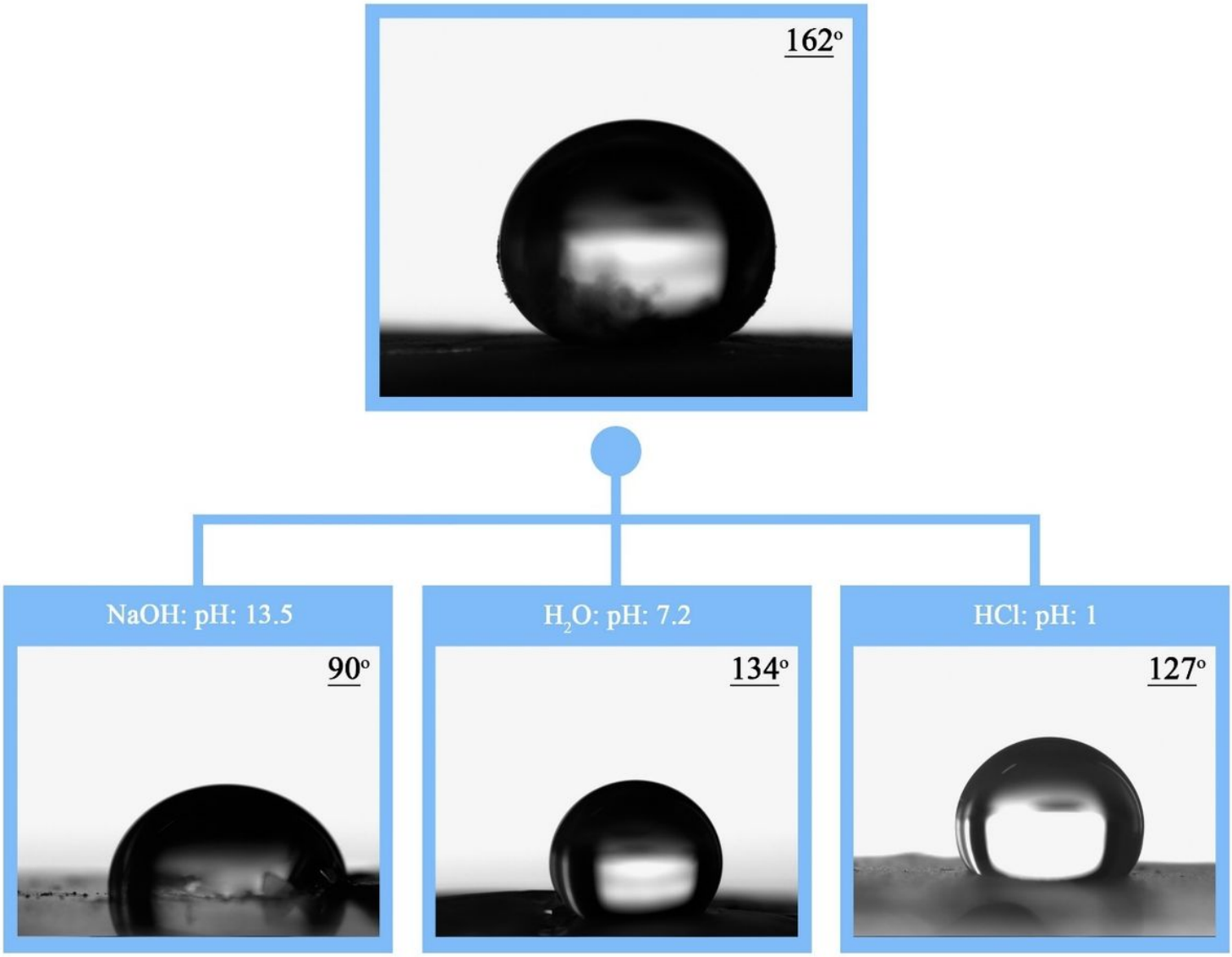

Figure 12

Effect of pH on the contact angle of the optimized sample

Supplementary Files

This is a list of supplementary files associated with this preprint. Click to download.

- supplementary1.docx
- floatimage13.jpeg